Direct measurement of the Kirkwood-Rihaczek distribution for the spatial properties of a coherent light beam

Viktor Bollen, Yong Meng Sua, and Kim Fook Lee*
Department of Physics, Michigan Technological University, Houghton, Michigan 49931, USA
(Received 9 February 2010; published 25 June 2010)

We present a direct measurement of the Kirkwood-Rihaczek (KR) distribution for spatial properties of a coherent light beam in terms of position and momentum (angle) coordinates. We employ a two-local oscillator (LO) balanced heterodyne detection (BHD) to simultaneously extract the distribution of the transverse position and momentum of a light beam. The two-LO BHD can measure the KR distribution for any complex wave field (including quantum mechanical wave function) without applying tomography methods (inverse Radon transformation). The transformation of the KR distribution to the Wigner, Glauber-Sudarshan P, and Husimi or Q distributions in spatial coordinates are illustrated through experimental data. The KR distribution can provide the local information of a wave field, which is suitable for studying particle properties of a quantum system. Meanwhile, the Wigner function is suitable for studying wave properties such as interference, and hence provides nonlocal information of the wave field. The method developed here can be used for exploring the spatial quantum state for information processing and optical phase-space imaging for biomedical applications.

DOI: 10.1103/PhysRevA.81.063826 PACS number(s): 42.50.Ar, 42.25.Kb, 87.57.C−, 42.50.Ex

I. INTRODUCTION

Optical phase-space tomography [1–8] is an imaging optical method for characterizing spatial properties of the light field or photon. The Kirkwood [K(x,p)] [9] and Wigner [W(x,p)] [10] distribution functions were originally proposed in the studies of quantum statistics and thermodynamics for almost classical ensembles. The Kirkwood distribution [$\psi(x)\psi^*(p)e^{-ixp}$] has been rediscovered by Rihaczek [11] for use in the theory of time-frequency analysis of classical signals. The Wigner function is more popular than the Kirkwood-Rihaczek (KR) function because it has some unique properties such as negative values, real, and symmetry. It can be obtained through tomograph methods and is applicable to problems in the phase-space transport equation such as the Liouville equation [12]. The Wigner function was first introduced in the optical light field by Bastiaans [13,14] to analyze spatial properties of an optical Gaussian beam. In quantum optics, the quantum mechanical wave function cannot be measured. The wave function or quantum state of a physical system can be best represented by the Wigner function. Vogel and Risken [15] had theoretically proposed how quadrature amplitudes of nonclassical light fields can be represented in the Wigner distribution by tomograph methods. Raymer [16–20] has pioneered the tomography measurement of the Wigner function for quadrature amplitudes of squeezed light, spatial properties, and time-frequency properties of coherent light (a coherent state with a large mean photon number). The KR and Wigner distributions can be reconstructed from the wave front of a wave field. A wave-front sensor such as the Shack-Hartmann sensor [21] consisting of a diode array can directly measure the wave front of a wave field. However, the technique has a disadvantage compared to optical balanced detection, which can be used to measure the spatial properties of a nonclassical light field (i.e., below shot-noise level).

The Glauber-Cahill s-parameterized class of quasidistributions [22] that contain the Wigner function, the Glauber-Sudarshan P representation [23], and the Husimi [24] or the Q representation have been widely used as powerful phase-space tools. However, most of the tomograph methods such as optical balanced homodyne detection and wave-front sensing do not involve direct measurement of these quasiquantum distribution functions. These distributions are usually reconstructed from the raw data, where numerical and mathematical transformation discrepancies may have made these distributions doubtful for representing the true states. The direct measurement of these distributions is desirable to represent the true quantum state. It is well understood that tomograph methods developed for these distributions can be used for any complex wave field regardless of classical or quantum origin [17,25]. In this perspective, we use wave field to represent the quantum mechanical wave function and coherent light field.

The KR distribution for any quantum state in a generalized form has been introduced [26]. It is worth noting that the position and momentum distributions of the wave field can be obtained through the KR distribution such as $\int K(x,p)dp = |\psi(x)|^2$ and $\int K(x,p)dx = |\psi(p)|^2$, respectively. These properties are similar to the Wigner function. Moreover, the complex conjugated KR can be directly measured through a two-local oscillator (LO) technique [1], not like the Wigner function, which is reconstructed from experimental data using quantum tomographic methods. The phase-space distribution functions, especially the Wigner function, can unravel unique quantum properties such as entanglement of correlated systems [27,28], negative parts of the phase-space plots [29], and the phase space sub-Planck structures of quantum interference [30,31]. The KR function is relatively unexplored for quantum fields.

In the second quantization of quantum mechanics, the electric field is written as an operator in terms of the harmonic oscillator basis, that is, position and momentum operators. The spatial property of the electric field perpendicular to the propagation direction is described by mode functions. The

*kflee@mtu.edu

mode function in an x or p coordinate is a description of the probability amplitude to find a photon at transverse position x or transverse momentum p, respectively. The field operator $\hat{a}(x)$ corresponding to the mode function will provide mean field $\langle\hat{a}(x)\rangle$ and quantum noise $\triangle\hat{a}(x)$ in an optical detection scheme. The mean value measurement of the wave field $\langle\hat{a}(x)\rangle$ at a configuration space will provide a classical-like feature regardless of the origin (classical or quantum light) of the measured field. A variance measurement of the wave field $\triangle\hat{a}(x)$ will provide a quantum feature of the light field. For a coherent state with a low or large mean photon number, the variance for the quantum noise of the wave field is constant [32], that is, position or momentum independence. Therefore, the measurement method we have developed for coherent light is also applicable to the coherent state, making them a useful testing ground for single-photon quantum imaging [7].

In most quantum information experiments, a single spatial mode of the electromagnetic field is generally used and considered [33,34]. Quantum fluctuations of light at different spatial points in the transverse plane of the light beam have to be taken into account. Kolobov and Sokolov [35–39] have studied in detail the possibility of local squeezing in a spatial mode of the light beam. Multimode spatial modes will cause information processing and computing errors. Spatial coherence of light sources is necessary for achieving efficient coupling into fiber systems for quantum communication and also for biomedical imaging in image-guide intervention [40]. From a quantum-mechanical perspective, the spatial degree of freedom of a photon is another optical quantum realization for encoding information such as spatial qubits [33]. A full characterization of arbitrary, continuous spatial states of photons is important for understanding the concept of the photon wave function [25]. The Wigner function for an ensemble of identically prepared photons in the transverse spatial modes can be completely used to characterize the transverse spatial state of the ensemble. Recently, the Einstein-Podolsky-Rosen (EPR) entanglement in a spatial coordinate has been demonstrated by mixing an optical coherent light beam with squeezed light [41]. However, their measurements involved displacement and "tilt" (momentum or angular) of a whole optical beam, not the transverse amplitude and phase structure of the optical beam. The KR distributions are relatively unexplored for spatial properties of wave fields.

Phase-space distributions are used to represent quantum-mechanical operators in exploring phase-space quantum effects and quantum-classical correspondence. Quantum algorithms for measuring the KR and Wigner distributions have been developed [42,43]. Discrete phase-space distribution has been suggested to show the potential advantages in quantum computing, especially quantum mapping. A quantum algorithm can be simply thought of as a quantum map acting in a Hilbert space of finite dimensionality. Specifically, algorithms become interesting in the large-N limit (i.e., when operating on many qubits). For a quantum map, this is the semiclassical limit where regularities may arise in connection with its classical behavior. These semiclassical properties may provide hints to develop new algorithms and ideas for novel physics simulations.

In this paper, we demonstrate the direct measurement of the KR distribution for a wave field with a Gaussian mode function of TEM_{00}. The linear transformation from the KR distribution to the Wigner, P, and Q distributions are also plotted to show their respective fundamental differences. Then a superposition of two spatially separated coherent light beams is used for discussing the phase-space interferences in these distributions. We show that complex conjugated KR distributions for spatial properties of wave fields can be determined by the use of a novel two-LO balanced heterodyne detection scheme [1]. The technique measures $\mathcal{K}^*(x,p) =< \mathcal{E}^*(x)\mathcal{E}(p) > e^{ixp}$, which can be written as $S_R + iS_I$. A lock-in amplifier is used to measure the S_R and S_I with respect to the relative phase setting of a reference signal at 0° and 90°, respectively. By changing the lock-in-amplifier reference phases such as 0° and -90°, the system will measure $\mathcal{K}(x,p)$. However, we keep the lock-in amplifier with reference phases at 0° and 90° for all measurements in this paper. There is no different in the physics implied by the wave field in the KR or complex conjugated KR representation. The two-LO heterodyne technique was originally designed for biomedical imaging, that is, for optical phase-space coherence tomography of the light transmitted through or reflected from biological tissue. Now we use this measurement to explore the properties of one-particle wave mechanics or the wave field through the KR, Wigner, P, and Q distributions. The technique can be used to measure any complex spatial wave fronts such as divergence and convergence and phase-conjugated properties of a wave field [3,4]. The $\mathcal{K}^*(x,p)$ can be easily transformed to the Wigner function by using a linear transformation where the Radon transform is not required. The advantage of the KR is that it contains local information of the wave field. If there is no wave field present at a configuration space (x,p), then there will be no distribution at the (x,p). This serves us better for optical imaging in biomedical applications such as for characterizing the cell structure. We will illustrate this spatial property of the KR distribution and compare it with the Wigner function, P, and Q distributions. In the two-LO balanced heterodyne detection, we use an LO field comprising a coherent superposition of a tightly focused LO Gaussian beam of TEM_{00} and a highly collimated LO Gaussian beam of TEM_{00}. This scheme permits independent control of the x and p resolutions, permitting concurrent localization of x and p with a variance product that surpasses the minimum uncertainty limit associated with Fourier-transform pairs. Quantum mechanics does not allow for the simultaneous measurement of x and p of a wave field. However, simultaneous measurement in the distribution of x and p for a wave field is allowed.

II. CHARACTERISTIC FUNCTION APPROACH

In this section, the characteristic function method [44,45] will be used to transform the characteristic function of the KR distribution to the Wigner, P, and Q distributions. The characteristic functions in terms of the harmonic oscillator basis will be used throughout this paper because they are more revelent to the spatial properties of coherent wave fields. Since we directly measure the complex conjugated KR distribution, we will discuss how experimental data can be used to obtain the Wigner, P, and Q distributions. We start with the characteristic function for the complex conjugated KR distribution in terms of a coherent state representation, as given by

$$\mathcal{M}_{\mathrm{KR}}(\beta,\beta^*) = \mathrm{Tr}\,(\rho e^{-|\beta^2-\beta^{*2}|/4} e^{i\beta\hat{a}^\dagger + i\beta^*\hat{a}}), \qquad (1)$$

where (β,β^*) are the Fourier conjugate pairs for (α, α^*) the eigenvalues of $\hat{a}$ and $\hat{a}^*$, respectively. The interesting feature of this characteristic function in the Fourier plane $M_{\rm KR}(\beta,\beta^*)$ is the trace of the displacement operator $\hat{\mathcal{D}}(\beta)$ followed by the squeezing operator $\mathcal{S}(1/2)$. The absolute of $|\beta^2-\beta^{*2}|/4$ is used just to avoid the confusion of other forms of the definition such that $\beta \rightarrow i\beta$ and $\beta^* \rightarrow -i\beta^*$. The complex conjugated KR distribution in the (α,α^*) plane can be obtained through

$$\mathcal{K}^*(\alpha,\alpha^*) = \frac{1}{\pi^2}\int d^2\beta e^{-i\beta\alpha^*-i\beta^*\alpha}\mathcal{M}_{\rm KR}(\beta,\beta^*). \tag{2}$$

The $\mathcal{K}^*(\alpha,\alpha^*)$ can be transformed to the Wigner, P, and Q distributions in terms of (α,α^*) through the relationships of the characteristic functions, such that

$$\mathcal{M}_{\rm KR}(\beta,\beta^*) = e^{-|\beta^2-\beta^{*2}|/4}\mathcal{M}_W(\beta,\beta^*), \tag{3}$$

where

$$\mathcal{M}_W(\beta,\beta^*) = e^{-|\beta|^2/2}\mathcal{M}_P(\beta,\beta^*) = e^{|\beta|^2/2}\mathcal{M}_Q. \tag{4}$$

The characteristic function for the Wigner function is given by

$$\mathcal{M}_W(\beta,\beta^*) = {\rm Tr}(\rho e^{i\beta\hat{a}^\dagger+i\beta^*\hat{a}}). \tag{5}$$

The P and Q representations are related to the characteristic function of the Wigner function through normal ordering and antinormal ordering of $(\hat{a},\hat{a}^*)$.

In our experiment, we measure the spatial properties of a wave field in terms of the position and momentum coordinates (x,p). Then, the transformation of $\mathcal{K}^*(\alpha,\alpha^*) \rightarrow \mathcal{K}^*(x,p)$ can be obtained from Eqs. (1) and (2) using the variables

$$\begin{aligned}
\hat{a} &= \frac{1}{\sqrt{2}}(\hat{x}+i\hat{p}); \quad \hat{a}^\dagger = \frac{1}{\sqrt{2}}(\hat{x}-i\hat{p}),\\
\beta &= \frac{1}{\sqrt{2}}(\sigma+i\tau); \quad \beta^* = \frac{1}{\sqrt{2}}(\sigma-i\tau),\\
\sigma &= \frac{1}{\sqrt{2}}(x+ip); \quad \sigma^* = \frac{1}{\sqrt{2}}(x-ip).
\end{aligned} \tag{6}$$

Then the following terms,

$$\begin{aligned}
e^{i\beta\hat{a}^\dagger+i\beta^*\hat{a}} &= e^{i\sigma\hat{x}+i\tau\hat{p}},\\
e^{-|\beta^2-\beta^{*2}|/4} &= e^{-i\sigma\tau/2},\\
e^{-i\beta\sigma^*-i\beta^*\sigma} &= e^{-i\sigma x-i\tau p},
\end{aligned} \tag{7}$$

are obtained. The $\mathcal{K}^*(x,p)$ can be written as

$$\mathcal{K}^*(x,p) = \int d\sigma d\tau e^{-i\sigma x-i\tau p}{\rm Tr}(\rho e^{i\sigma\hat{x}+i\tau\hat{p}}e^{i\sigma\tau}). \tag{8}$$

By using the identity $\int dx|x\rangle\langle x| = \hat{1}$ and $\hat{\rho} = |\psi\rangle\langle\psi|$, we obtain

$$\mathcal{K}^*(x,p) = \frac{2}{\pi}\psi^*(x)\int e^{-i\tau p}\psi(x+\tau)d\tau. \tag{9}$$

By changing the variable $\xi = x+\tau$, $d\xi = d\tau$, we obtain

$$\mathcal{K}^*(x,p) = \frac{2}{\pi}\psi^*(x)\psi(p)e^{ixp}, \tag{10}$$

which is the complex conjugated KR distribution. To write the characteristic functions of the Wigner, P, and Q distributions in terms of the spatial properties of a coherent light beam such as beam waist σ and position and momentum coordinates (x,p), we use the variables

$$\beta = \frac{1}{\sqrt{2}}(p'\sigma - ix'/\sigma); \quad \beta^* = \frac{1}{\sqrt{2}}(p'\sigma + ix'/\sigma),$$

so that the characteristic functions for the KR, Wigner, P, and Q distributions are related to each other as given by

$$\mathcal{M}_{\rm KR}(x',p') = e^{-ix'p'/2}\mathcal{M}_W(x',p'), \tag{11}$$

and

$$\begin{aligned}
\mathcal{M}_W(x',p') &= e^{-\frac{1}{4}(\sigma^2p'^2+x'^2/\sigma^2)}\mathcal{M}_P(x',p')\\
&= e^{\frac{1}{4}(\sigma^2p'^2+x'^2/\sigma^2)}\mathcal{M}_Q(x',p').
\end{aligned} \tag{12}$$

Since our experiment measures the $\mathcal{K}^*(x,p)$, its characteristic function is obtained through the transformation as given by

$$\mathcal{M}_{\rm KR}(x'p') = \int dxdp\mathcal{K}^*(x,p)e^{ixp'+ipx'}. \tag{13}$$

Then the Wigner function is obtained through

$$W(x,p) = \int dx'dp'e^{ix'p'/2}\mathcal{M}_{\rm KR}(x',p')e^{-ixp'-ipx'}, \tag{14}$$

or in the simplified form as in Ref. [1],

$$W(x,p) = \frac{1}{\pi}\int dx'dp'e^{-2i(x'-x)(p'-p)}\mathcal{K}^*(x',p'). \tag{15}$$

Similarly, the P and Q distributions can be obtained through

$$\begin{aligned}
P(x,p) = \int & e^{ix'p'/2}\mathcal{M}_{\rm KR}(x',p')e^{\frac{1}{4}(\sigma^2p'^2+x'^2/\sigma^2)}\\
&\times e^{-ixp'-ipx'}dx'dp',
\end{aligned} \tag{16}$$

and

$$\begin{aligned}
Q(x,p) = \int & e^{ix'p'/2}\mathcal{M}_{\rm KR}(x',p')e^{-\frac{1}{4}(\sigma^2p'^2+x'^2/\sigma^2)}\\
&\times e^{-ixp'-ipx'}dx'dp',
\end{aligned} \tag{17}$$

respectively.

The similarity of the KR and Wigner functions is that when they are integrated over momentum or position, the two functions will provide the same result for the probability in position or momentum [i.e., $\int \mathcal{K}^*(x,p)dx = \int W(x,p)dx = |\psi(p)|^2$ and $\int \mathcal{K}^*(x,p)dp = \int W(x,p)dp = |\psi(x)|^2$]. It should be noted that because of the uncertainty principle, neither function has a physical meaning until it is integrated over either momentum space or configuration space.

III. EXPERIMENT DETAILS

Since tomography methods developed for spatial properties of the photon wave function can be applied to the coherent field (coherent state with large mean photon number), we use electric field notation $\mathcal{E}(x)$ to represent the wave field $\psi(x)$ in the following sections.

We use a balanced heterodyne detection scheme as shown in Fig. 1. The beat amplitude V_B is determined by the spatial overlap of the LO and signal (S) fields in the plane of the detector at $Z = Z_D$ as

$$V_B = \int dx'\mathcal{E}^*_{\rm LO}(x',z_D)\mathcal{E}_S(x',z_D), \tag{18}$$

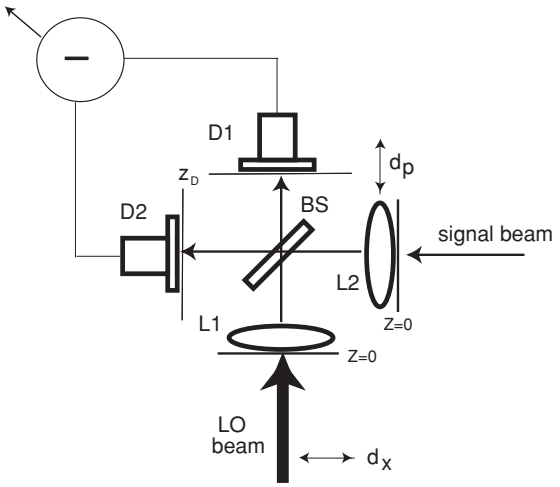

FIG. 1. A balanced heterodyne optical phase-space imaging scheme.

where x' denotes the transverse position in the detector plane. When the LO beam is moved by a distance d_x, the V_B becomes

$$V_B(d_x) = \int dx' \mathcal{E}^*_{\mathrm{LO}}(x' - d_x, z_D)\mathcal{E}_S(x', z_D). \tag{19}$$

The fields in the detector plane are related to the fields in the source planes ($z = 0$) of lenses L1 and L2, which have equal focal lengths of $f = 6$ cm. The LO and signal fields at $z = 0$ after the lenses, L1 and L2, are given by [46]

$$\begin{aligned} \mathcal{E}'_{\mathrm{LO}}(x_1 - d_x, z = 0) &= \exp\left[-i\frac{k}{2f}x_1^2\right]\mathcal{E}_{\mathrm{LO}}(x_1 - d_x, z = 0), \\ \mathcal{E}'_S(x_2, z = 0) &= \exp\left[-i\frac{k}{2f}x_2^2\right]\mathcal{E}_S(x_2, z = 0). \end{aligned} \tag{20}$$

When the lens L2 is scanned by a distance d_p, the signal field (20) is altered as

$$\mathcal{E}'_S(x_2, z = 0) = \exp\left[-i\frac{k}{2f}(x_2 - d_p)^2\right]\mathcal{E}_S(x_2, z = 0).$$

The fields propagating a distance $d = f$ to the planes of the detectors can be obtained by using Fresnel's diffraction integrals as

$$\begin{aligned} \mathcal{E}_{\mathrm{LO}}(x' - d_x, z_D) = \sqrt{\frac{k}{i2\pi f}} \int dx_1 \exp\left[i\frac{k}{2f}(x_1 - x')^2\right] \\ \times \exp\left[-i\frac{k}{2f}x_1^2\right]\mathcal{E}_{\mathrm{LO}}(x_1 - d_x, z = 0), \\ \mathcal{E}_S(x', z_D) = \sqrt{\frac{k}{i2\pi f}} \int dx_2 \exp\left[i\frac{k}{2f}(x_2 - x')^2\right] \\ \times \exp\left[-i\frac{k}{2f}(x_2 - d_p)^2\right]\mathcal{E}_S(x_2, z = 0). \end{aligned} \tag{21}$$

By substituting the above equations into Eq. (19), the quadratic phases in x' cancel and the quadratic phases that depend on $x_{1,2}^2$ cancel in these expressions because the detector plane is in the focal plane of the lenses, L1 and L2. One obtains

$$\begin{aligned} V_B(d_x, d_p) = \frac{k}{f}\exp\left[i\frac{k}{2f}d_p^2\right] \\ \times \int dx_2 \exp\left[-i\frac{k}{f}x_2 d_p\right]\mathcal{E}_S(x_2, z = 0) \\ \times \int dx_1 \mathcal{E}^*_{\mathrm{LO}}(x_1 - d_x, z = 0)\delta(x_1 - x_2). \end{aligned} \tag{22}$$

Integrating over x_1 and by replacing x_2 by x and dropping the term $z = 0$, the mean square beat amplitude is then given by

$$|V_B(d_x, d_p)|^2 \propto \left|\int dx \mathcal{E}^*_{\mathrm{LO}}(x - d_x)\mathcal{E}_S(x)\exp\left(-ik\frac{d_p}{f}x\right)\right|^2,$$

or

$$\begin{aligned} |V_B(d_x, d_p)|^2 \propto \int dx \mathcal{E}^*_{\mathrm{LO}}(x - d_x)\mathcal{E}_S(x)\exp\left(-ik\frac{d_p}{f}x\right) \\ \times \int dx' \mathcal{E}_{\mathrm{LO}}(x' - d_x)\mathcal{E}^*_S(x')\exp\left(ik\frac{d_p}{f}x'\right). \end{aligned} \tag{23}$$

This can be rewritten using the variable transformations $x = x_o + \eta/2$; $x' = x_o - \eta/2$ where the Jacobian of this transformation is 1. Then, by using the definition of the Wigner distribution,

$$W(x, p) = \int \frac{d\epsilon}{2\pi}\exp(i\epsilon p)\langle\mathcal{E}^*(x + \epsilon/2)\mathcal{E}(x - \epsilon/2)\rangle, \tag{24}$$

and its inverse transform is given by

$$\mathcal{E}^*(x_0 + \epsilon/2)\mathcal{E}(x_0 - \epsilon/2) = \int dp \exp(-i\epsilon p)W(x_0, p), \tag{25}$$

the beat signal in Eq. (23) becomes

$$\begin{aligned} |V_B(d_x, d_p)|^2 \propto \int dx_0 \int d\eta \mathcal{E}^*_{\mathrm{LO}}(x_0 + \eta/2 - d_x) \\ \times \mathcal{E}_{\mathrm{LO}}(x_0 - \eta/2 - d_x)\int dp \exp\left(-ik\frac{d_p}{f}\eta\right) \\ \times \exp(-i\eta p)W_S(x_0, p). \end{aligned} \tag{26}$$

Since the Wigner distribution of the LO field is

$$\begin{aligned} W_{\mathrm{LO}}\left(x_0 - d_x, p + k\frac{d_p}{f}\right) \\ = \int \frac{d\eta}{2\pi}\exp\left[-i\eta\left(p + k\frac{d_p}{f}\right)\right]\mathcal{E}^*_{\mathrm{LO}}(x_0 + \eta/2 - d_x) \\ \times \mathcal{E}_{\mathrm{LO}}(x_0 - \eta/2 - d_x), \end{aligned} \tag{27}$$

then the LO fields in Eq. (26) can be replaced by the Wigner function in Eq. (27). Finally, the mean square heterodyne beat signal $|V_B|^2$ can now be written as

$$|V_B(d_x, d_p)|^2 \propto \int dx dp W_{\mathrm{LO}}\left(x - d_x, p + k\frac{d_p}{f}\right)W_S(x, p), \tag{28}$$

where we have applied $x_0 \to x$. The $W_S(x, p)$ is the Wigner distribution of the signal field in the plane of L2 ($z = 0$) and

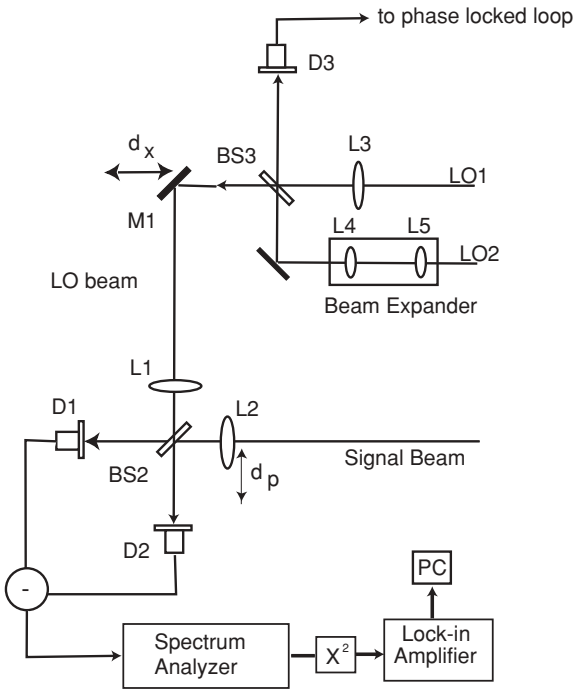

FIG. 2. Experimental setup for measuring the KR distribution using two-LO balanced heterodyne detection. X^2; squarer, D; photodiode detector, BS; beam splitter.

$W_{\mathrm{LO}}(x,p)$ is the LO Wigner distribution in the plane of L1 ($z=0$). We include a detailed description of the two-window heterodyne measurement of the KR distribution as shown in Fig. 2. The variables d_x and d_p, respectively, indicate the positions of a mirror M1 and a lens L2, respectively, as shown in Fig. 2. Equation (28) shows that the mean-square beat signal yields a phase-space contour plot of $W_S(x,p)$ with the phase-space resolution determined by $W_{\mathrm{LO}}(x,p)$. By using a two-LO heterodyne detection scheme as discussed in the following, the $|V_B(d_x,d_p)|^2$ is found to be proportional to $\mathcal{K}^*(x,p)$.

To obtain independent control of the x and p resolutions in the heterodyne measurement, we employ a slowly varying LO field containing a focused and a collimated field with a well-defined relative phase θ

$$\mathcal{E}_{\mathrm{LO}}(x)=\mathcal{E}_0\left[\exp\left(-\frac{x^2}{2a^2}\right)+\alpha\exp\left(-\frac{x^2}{2A^2}\right)\exp(i\theta)\right]. \tag{29}$$

Here a is chosen to be small compared with the distance scales of interest and $1/A$ is chosen to be small compared with the momentum scales of interest in the signal field. The schematic picture of the overlapping of the LO beam with the spatial width a and another LO beam with the spatial width A is shown in Fig. 3. One can see that the overlapping area is determined by the position and momentum resolutions for the LO fields in Eq. (29). The focused LO Gaussian beam extracts the position information of the signal field and the collimated LO Gaussian beam extracts the momentum information of the signal field. The Wigner function for the LO field is obtained by substituting Eq. (29) into Eq. (24). We take $A^2 \gg a^2$. In

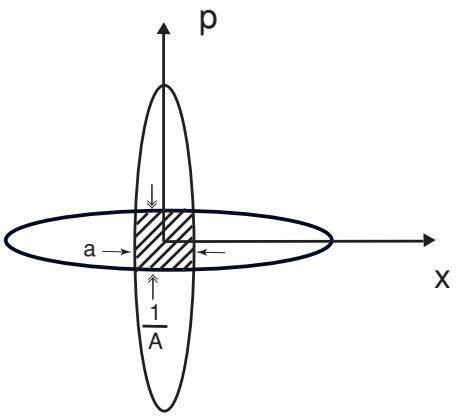

FIG. 3. The overlapping area is the position and momentum resolutions of the combined LO beams. The uncertainty is proportional to $\frac{a}{A}$ less than 1.

this case the phase-dependent (θ) part of the Wigner function for the LO takes the form

$$W_{\mathrm{LO}}(x,p)\propto\exp\left(-\frac{2x^2}{A^2}-2a^2p^2\right)\cos(2xp+\theta)$$
$$\simeq\cos(2xp+\theta), \tag{30}$$

where the last form assumes that the range of the momentum and position integration in relation (28) is limited by the signal field.

The measurement of the phase-space distributions is accomplished by the translation of optical elements. These elements are all mounted on translation stages driven by computer-controlled linear actuators. The system scans the LO position over a distance $d_x=\pm1$ cm by translating mirror M1 in the LO path. The LO momentum is scanned over $\pm0.3k$, where $k=2\pi/\lambda$ is an optical wave vector, by translation of the signal-beam input lens L2 (focal length $f=6$ cm) by a distance d_p.

In the experiments, as illustrated in Fig. 2, the LO beam is obtained by combination of two fields that differ in frequency by 5 kHz, so that $\theta=(2\pi\times5\ \mathrm{kHz})t$. Lens L3 focuses beam LO1 to a waist of width a, and lenses L4 and L5 expand beam LO2 to width A. We combine these two components at beam splitter BS3 to obtain an LO field of the form given in Eq. (29). We monitor one output of the beam splitter with detector D_3 to phase lock the 5 kHz beat signal to the reference channel of the lock-in amplifier. Each component of the LO beam is shaped so that it is at a beam waist at the input plane of the heterodyne imaging system (lens L1). The focused Gaussian LO beam is frequency shifted at 110 MHz and the collimated Gaussian LO beam is frequency shifted at 110 MHz plus 5 kHz. These two LO beams are overlapped with each other and phase locked at 5 kHz. The signal beam is frequency shifted at 120 MHz. Two imaging lenses L1 and L2 are used to overlap the dual LO beam with the signal beam at two detectors. The interference beat signal between the signal beam and the dual LO beam is obtained at detectors 1 and 2 and consists of 10 MHz and 10 MHz plus 5 kHz components. These signals are sent to a spectrum analyzer. The spectrum analyzer bandwidth, 100 kHz, is chosen to be large compared with the 5 kHz difference frequency. The output of the analyzer

is then squared by using an analog multiplier. The mean square signal has components at 5 kHz. A lock-in amplifier is used to measure the in-phase and out-of phase components of the multiplier output at 5 kHz. The lock-in outputs for in-phase and out-of-phase quadratures then directly determine the real and the imaginary parts of the $\mathcal{K}^*(x,p)$ function

$$\begin{aligned}|V_B(d_x,d_p)|^2 &= \mathcal{K}^*(x_0,p_0)\\ &= \int \frac{dx'dp'}{\pi}\exp[2i(x'-x_0)(p'-p_0)]W_S(x',p')\\ &= \langle \mathcal{E}^*(x_0)\mathcal{E}(p_0)\rangle \exp(ix_0p_0) = S_R + iS_I, \end{aligned} \quad (31)$$

where the $W_{\mathrm{LO}}(x,p)$ in Eq. (30) is replaced by $e^{i(2xp+\theta)}$ in Eq. (28) yielding the in-phase and out-of-phase contributions from θ. Here $x_0 = d_x$ is the center position of the LO fields and $p_0 = -kd_p/f$ is the center momentum. The S_R and S_I components are related to the heterodyne beat signal of $E^*_{\mathrm{LO1}}E_S$ and $E^*_{\mathrm{LO2}}E_S$ or intensity correlation of $E^*_{\mathrm{LO1}}E_SE^*_{\mathrm{LO2}}E_S$. In the balanced heterodyne detection, the output voltage $V_B(t) = V_1(t) - V_2(t)$ before being fed into the spectrum analyzer is given by

$$V_B(t) = 2E^*_SE_{\mathrm{LO1}}e^{-i(\Omega_{\mathrm{LO1}}-\Omega_S)t} + 2E^*_SE_{\mathrm{LO2}}e^{-i(\Omega_{\mathrm{LO2}}-\Omega_S)t} + \text{c.c.} \quad (32)$$

In the spectrum analyzer, the power spectrum of the V_B is measured as

$$|V_B(\Omega)|^2 = \int_{-\infty}^{\infty}\frac{d\tau}{2\pi}e^{i\Omega\tau}\langle V_B(t)V_B(t+\tau)\rangle. \quad (33)$$

As mentioned previously, it is squared by using a squarer to recover the beat signal $|V_B(\Omega)|^2$. From Eq. (33), the power spectrum can be calculated by keeping the slowly varying term $(\Omega_{\mathrm{LO1}} - \Omega_{\mathrm{LO2}})$ in time t and other terms that depend on τ, that is,

$$\begin{aligned}\langle V_B(t)V_B(t+\tau)\rangle &= \frac{1}{T}\int_{-T/2}^{T/2}dtV_B(t)V_B(t+\tau)\\ &\propto E^*_SE_{\mathrm{LO1}}E_SE^*_{\mathrm{LO1}}e^{-i(\Omega_S-\Omega_{\mathrm{LO1}})\tau} + E^*_SE_{\mathrm{LO2}}E_SE^*_{\mathrm{LO2}}e^{-i(\Omega_S-\Omega_{\mathrm{LO2}})\tau}\\ &\quad + E^*_SE_{\mathrm{LO1}}E_SE^*_{\mathrm{LO2}}e^{-i(\Omega_{\mathrm{LO1}}-\Omega_{\mathrm{LO2}})t}e^{-i(\Omega_S-\Omega_{\mathrm{LO2}})\tau} + E^*_SE_{\mathrm{LO2}}E_SE^*_{\mathrm{LO1}}e^{i(\Omega_{\mathrm{LO1}}-\Omega_{\mathrm{LO2}})t}e^{-i(\Omega_S-\Omega_{\mathrm{LO1}})\tau}\\ &\quad + (\text{the negative frequency contributions from the above terms}). \end{aligned} \quad (34)$$

Here $\Omega_S = 120$ MHz, $\Omega_{\mathrm{LO1}} = 110$ MHz + 5 kHz, and $\Omega_{\mathrm{LO2}} = 110$ MHz. Now, by substituting Eq. (34) into Eq. (33) to obtain the power spectrum for the beat V_B and setting the analyzer at 10 MHz with the bandwidth of 100 kHz, the $|V_\circ(t)|^2$ at 5 kHz after the recovery by the squarer is

$$|V_\circ(t)|^2 \propto E^*_SE_{\mathrm{LO1}}E_SE^*_{\mathrm{LO2}}e^{-i(\Omega_{\mathrm{LO1}}-\Omega_{\mathrm{LO2}})t} + \text{c.c.} \quad (35)$$

Here $\Omega_{\mathrm{LO1}} - \Omega_{\mathrm{LO2}} = 5$ kHz. The in-phase and out-of-phase components of the $|V_\circ(t)|^2$ at 5 kHz correspond to S_R and S_I in Eq. (31). Note that $E^*_SE_{\mathrm{LO1}}$ is integrated over the transverse plane as is $E_SE^*_{\mathrm{LO2}}$. It is worth noting that the component $E^*_SE_{\mathrm{LO1}}$ of Eq. (35) corresponds to the measurement of the position distribution in $\mathcal{K}^*(x_0,p_0)$ of Eq. (31) by the tightly focused LO1 beam. Similarly, the component $E_SE^*_{\mathrm{LO2}}$ of Eq. (35) indicates the measurement of the momentum distribution in $\mathcal{K}^*(x_0,p_0)$ of Eq. (31) by the collimated LO2 beam.

As the position of mirror M1 is scanned a distance d_x, the optical path lengths of the LO fields change. For the current experiments, the HeNe laser is a source, the change in path lengths is small compared with the Rayleigh length and the coherence length of the beams, so translating M1 simply changes the center position of the LO fields.

IV. RESULTS

A. Measurement of an optical Gaussian beam

1. Gaussian beam

As an initial demonstration of the capability of this system, we measure the $\mathcal{K}^*(x,p)$ function for an ordinary Gaussian beam. A one-dimensional wave field for a Gaussian beam of TEM_{00} and radii of curvature R is given by

$$\begin{aligned}\mathcal{E}(x) &\propto \exp\left(-\frac{x^2}{2\sigma^2} + i\frac{kx^2}{2R}\right)\\ &\propto \mathcal{A} + i\mathcal{B}, \end{aligned} \quad (36)$$

where the x is the transverse position and σ is the waist of the signal beam. The Fourier transform of $\mathcal{E}(x)$ is

$$\begin{aligned}\mathcal{E}(p) &\propto \exp\left[-\frac{p^2}{8\sigma^2\left(\frac{1}{2\sigma^2}\right)^2 + \left(\frac{k}{2R}\right)^2} - i\frac{kp^2}{8R\left(\frac{1}{2\sigma^2}\right)^2 + \left(\frac{k}{2R}\right)^2}\right]\\ &\propto \mathcal{C} + i\mathcal{D}. \end{aligned} \quad (37)$$

The complex conjugated KR distribution for this wave field can be written as

$$\begin{aligned}\mathcal{K}^*(x,p) &= (\mathcal{AC} + \mathcal{BD})\cos(xp) + (\mathcal{BC} - \mathcal{AD})\sin(xp)\\ &\quad + i[(\mathcal{AD} - \mathcal{BC})\cos(xp) + (\mathcal{AC} - \mathcal{BD})\sin(xp)]. \end{aligned} \quad (38)$$

The characteristic function $\mathcal{M}_{\mathrm{KR}}(x,p)$ is obtained from Eq. (11), where the characteristic function for the Wigner function for this wave field is given by

$$\begin{aligned}\mathcal{M}_W(x',p') &= \int \mathcal{E}^*\left(\eta - \frac{x'}{2}\right)\mathcal{E}\left(\eta + \frac{x'}{2}\right)e^{ip'\eta}d\eta\\ &= \int \mathcal{E}^*\left(\eta + \frac{p'}{2}\right)\mathcal{E}\left(\eta - \frac{p'}{2}\right)e^{ix'\eta}d\eta\\ &= \exp\left[-\frac{x'}{4\sigma^2} - \frac{\sigma^2}{4}\left(\frac{kx'}{R} + p'\right)^2\right]. \end{aligned} \quad (39)$$

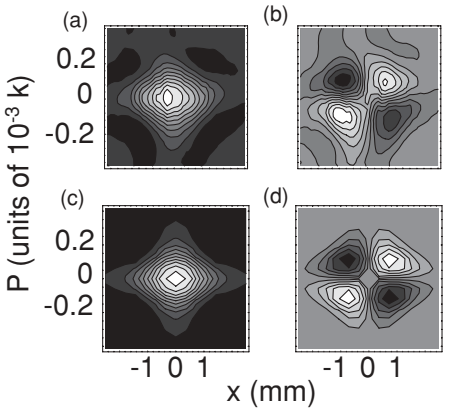

FIG. 4. The KR distribution for a Gaussian beam. Top row are the experimental results and bottom row is the theoretical prediction for a Gaussian beam. (a) and (c) In-phase component of $\mathcal{K}^*(x_0,p_0)$. (b) and (d) Out-of-phase component of $\mathcal{K}^*(x_0,p_0)$.

Then the Wigner, P, and Q distributions are obtained from Eqs. (14), (16), and (17), respectively. The Wigner function for the wave field is given by

$$W(x,p)=\frac{1}{\pi}\exp\left[-\frac{x^2}{\sigma^2}-\sigma^2\left(\frac{kx}{R}+p\right)^2\right]. \tag{40}$$

The P and Q distributions for the wave field are given in the integral form as

$$\begin{aligned}P(x,p)=&\int\exp\left(-\frac{\sigma^2k^2x'^2}{4R^2}-\frac{\sigma^2kx'p'}{2R}\right)\\&\times\exp(-ixp'-ipx')dx'dp'\\Q(x,p)=&\int\exp\left(-\frac{x'^2}{2\sigma^2}-\frac{\sigma^2p'^2}{2}-\frac{\sigma^2k^2x'^2}{4R^2}-\frac{\sigma^2kx'p'}{2R}\right)\\&\times\exp(-ixp'-ipx')dx'dp'.\end{aligned} \tag{41}$$

For simplicity, the signal Gaussian beam is shaped by a telescope so that its waist coincides with input plane L2 of the heterodyne imaging system. For a Gaussian beam at its waist, $R=\infty$, Eq. (38) gives the complex conjugated KR distribution as

$$\mathcal{K}^*(x,p)=\mathcal{AC}\cos(xp)+i\mathcal{AC}\sin(xp), \tag{42}$$

where $\mathcal{A}=\exp(-\frac{x^2}{2\sigma^2})$, $\mathcal{C}=\exp(-\frac{p^2\sigma^2}{2})$, and $\sigma=0.85$ mm is the $1/e$-intensity width. The $\mathcal{K}^*(x,p)$ function for the signal field is measured by use of the dual LO beam of the form given by Eq. (29) with $a=81$ μm, $A=2.6$ mm, and $\alpha=1$. The

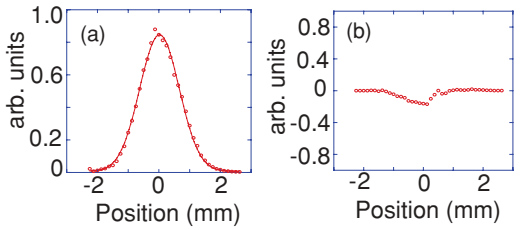

FIG. 5. (Color online) (a) Real part and (b) imaginary part of the position distribution of a Gaussian field. Imaginary part is around zero.

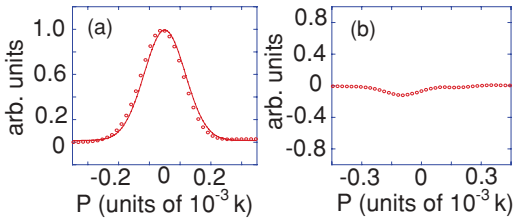

FIG. 6. (Color online) (a) Real part and (b) imaginary part of the momentum distribution of a Gaussian field. Imaginary part is around zero.

measurement result for a Gaussian beam is shown in Fig. 4. The top row are our experimental results and the bottom row is a theoretical prediction obtained by using Eq. (42). The real and the imaginary parts of the detected signal, Eq. (31), are shown in Fig. 4. Our observation is similar to the theoretical prediction by Wodkiewicz [26] for a coherent state.

Position (momentum) distributions of this field can be obtained through the summation of the momentum (position) coordinate of the real and the imaginary parts of the measured $\mathcal{K}^*(x,p)$. The position and momentum distributions are shown in Figs. 5 and 6, respectively. The imaginary part of the position and momentum distributions are around zero as theoretically predicted by $\int\mathcal{K}^*(x,p)dp=|\mathcal{E}(x)|^2$ and $\int\mathcal{K}^*(x,p)dx=|\mathcal{E}(p)|^2$, respectively, which are the real physical quantities (no complex values). From here, the position and momentum

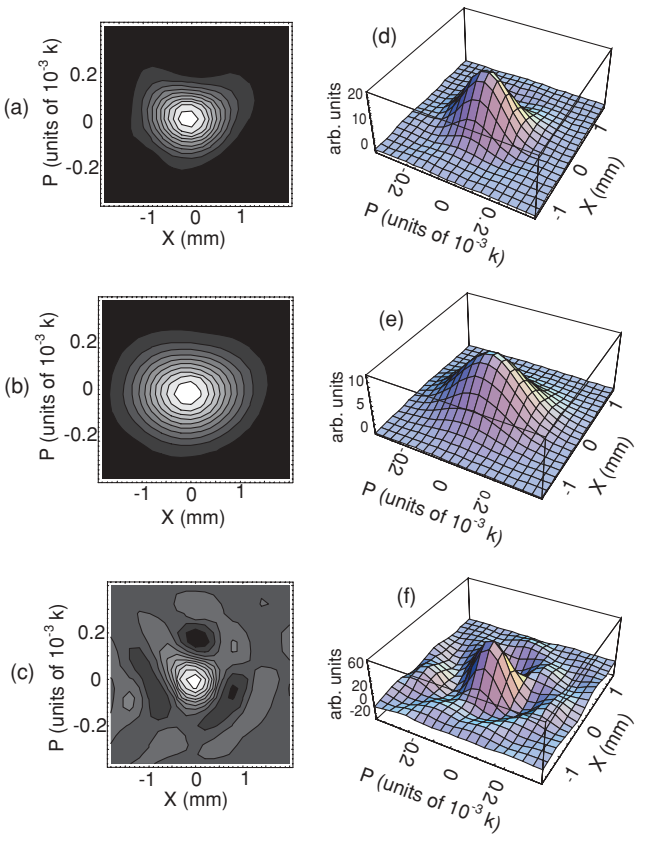

FIG. 7. (Color online) The reconstructed Wigner distribution (a) 2D plot (d) 3D plot, the Husimi or Q distribution (b) 2D plot (e) 3D plot, and the Glauber Sudarshan P distribution (c) 2D plot (f) 3D plot for an optical Gaussian beam.

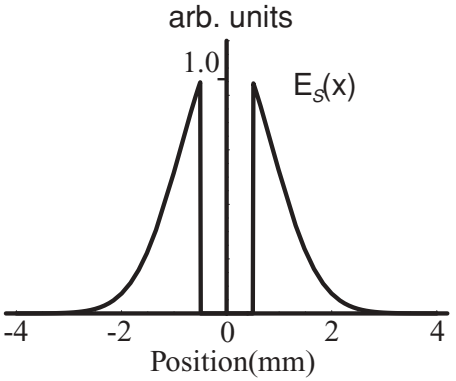

FIG. 8. The wave field $\mathcal{E}_S(x)$ of a Gaussian beam obscured by a wire.

distributions are fitted with a Gaussian function. We obtain the beam waist of $\sigma = 0.86$ mm from the position distribution and $\sigma = 0.87$ mm from the momentum distribution. Both results are in excellent agreement with the measured width $\sigma = 0.85$ mm obtained by use of a diode array, demonstrating that high position and momentum resolutions can be jointly obtained.

The Wigner distribution is obtained by using a simple linear transformation as discussed in Eqs. (14) or (15) and as shown in Figs. 7(a) [two-dimensional (2D) plot) and 7(d) [three-dimensional (3D) plot]. We χ^2 fit the width of the reconstructed Wigner function in position for $p = 0$ to obtain

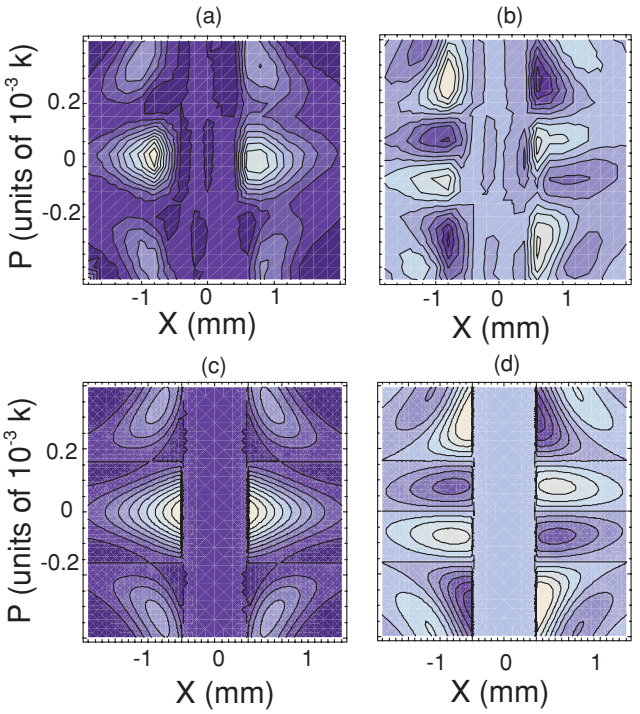

FIG. 9. (Color online) The KR distribution for two slightly displaced coherent beams. Top row shows the experimental results and the bottom row shows the theoretical predictions for a Gaussian beam blocked by a wire. (a) and (c) In-phase component of the $\mathcal{K}^*(x_0, p_0)$. (b) and (d) Out-of-phase component of the $\mathcal{K}^*(x_0, p_0)$.

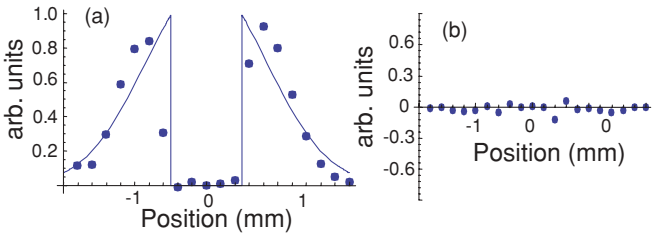

FIG. 10. (Color online) (a) The real part and (b) the imaginary part of the position distribution of a wire function obtained by integrating the measured KR distribution over momentum. Imaginary part is around zero.

a spatial width $\sigma = 0.87$ mm, whereas the corresponding momentum distribution for $x = 0$ yields $\sigma = 0.83$ mm.

The characteristic function $\mathcal{M}_{\mathrm{KR}}(x', p')$ is obtained by using the numerical integration of the measured $\mathcal{K}^*(x.p)$ as in Eq. (13). The Q and P distributions for this signal Gaussian beam are then obtained through Eqs. (17) and (16), as shown in Figs. 7(b) (2D plot) and 7(e) (3D plot) and Figs. 7(c) (2D plot) and 7(f) (3D plot), respectively. The P distribution has a narrower peak in phase space compared to the other distributions. This is predicted for the signal beam with $R = \infty$ in the P distribution of Eq. (41), which should have $\delta(x)\delta(p)$ in phase space. The Q distribution has a broad peak in phase space compared to the other distributions. The Q distribution for this signal beam can be evaluated from Eq. (41) with $R = \infty$, as given by

$$Q(x, p) \propto \exp\left(-\frac{p^2\sigma^2}{2} - \frac{x^2}{2\sigma^2}\right). \tag{43}$$

The position width of the Q distribution at $p = 0$ is about $\sqrt{2}$ larger than the position width of Wigner distribution at $p = 0$ as from Eq. (40). Hence the beam waist for the signal beam obtained from the Q distribution is $\sqrt{2}$ larger than the exact value.

2. *Measurement of superposition of two slightly displaced coherent beams*

As a fundamental feature in the process of quantum measurement, we cannot observe physical properties of a quantum objects directly because the overall backaction of any observation cannot be made less than Planck's constant h. Instead, we observe the wave or the particle aspects of the

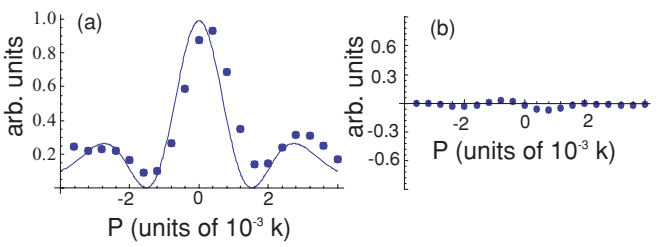

FIG. 11. (Color online) (a) The real part and (b) the imaginary part of the momentum distribution of a wire function obtained by integrating the measured KR distribution over position. Imaginary part is around zero.

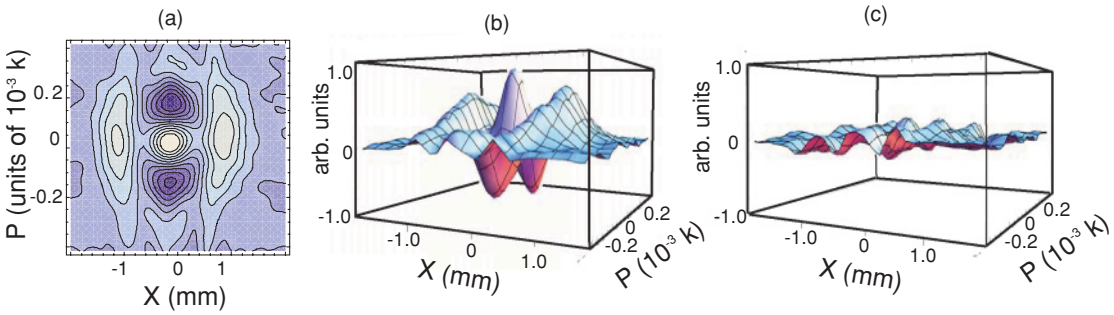

FIG. 12. (Color online) The reconstructed Wigner distribution for a wire function (a) 2D plot, (b) 3D plot, and (c) the imaginary part of the reconstructed Wigner function is around zero.

physical objects. The $\mathcal{K}^*(x,p)$ distribution for a coherent field more likely represents the particle picture of the field because it contains local information of the coherent field. While the Wigner function more likely represents the wave behavior of the field because it exhibits phase-space interference. Based on these properties, the $\mathcal{K}^*(x,p)$ and Wigner distributions are very useful in characterizing a wave field or a physical object through phase-space imaging in many applications such as quantum imaging, metrology, and biomedical imaging. To illustrate the particle picture of $\mathcal{K}^*(x,p)$ and the wave picture of the Wigner function, we use the same signal Gaussian beam obscured by a wire with a diameter of 1 mm. Then the electric field $\mathcal{E}_s(x)$ as a function of position is shown in Fig. 8. It does not involve convolution integration because the wire is placed close to the imaging lens L2. It shows the superposition of two slightly displaced coherent beams. It is analogous to a Schrödinger's cat state. In this case, the slowly varying field is Gaussian as before, but multiplied by a slit function that sets the field equal to zero for $|x| \leqslant 0.5$ mm. Figure 9 shows the contour plots of the real and the imaginary parts of the detected signal of $\mathcal{K}^*(x,p)$. The top row are our experimental results. The bottom row is the theoretical prediction. The theoretical plots are first obtained by numerically generating the signal function $\mathcal{E}_S(x)$ and its Fourier transform $\mathcal{E}_S(p)$. The real and imaginary parts of $\mathcal{K}^*(x,p)$ in Eq. (10) are then theoretically plotted. The real and imaginary parts are not showing phase-space interferences of two slightly displaced coherent beams. These plots show local information of the signal field [i.e., the zero (nonzero) field is corresponding to the zero (nonzero) $\mathcal{K}^*(x,p)$ phase-space distribution]. This locality property exhibits a particle picture if an atomic wave function or single photon function is used. The position and momentum distributions are then retrieved $\int \mathcal{K}^*(x,p)dp$ and $\int \mathcal{K}^*(x,p)dx$ as shown in Figs. 10 and 11, respectively. The momentum distribution contains the interference features of two spatially separated wave packets of $\mathcal{E}_S(x)$ as shown in Fig. 11. The imaginary part of these distributions is around zero as expected.

The Wigner function as shown in Fig. 12 is reconstructed by using the linear transformation of the measured $\mathcal{K}^*(x,p)$. The Wigner function is a real function. The reconstructed Wigner function should not have an imaginary part as shown in Fig. 12(c). The imaginary part is caused by the measurement errors in the experiment. The coherence between these two wave packets in the signal field leads to a phase-space interference pattern in the momentum distribution. The signature of this coherence in the Wigner distribution is the oscillating positive and negative values between the main lobes. An interesting feature of this Wigner distribution is the oscillation in momentum at the position $x = 0$ of the wire. We observe the negative values which are analogous to quantum interference in phase space. This feature can be seen in Fig. 12 in which the reconstructed Wigner function is shown as a three-dimensional plot. The negative values highlight the impossibility of a particle simultaneously having a precise position and momentum. It also makes sure that the sum over the momentum along $x = 0$ in the reconstructed Wigner distribution has zero intensity at the center. The negative and positive parts of the Wigner phase-space distribution are important features to obtain full information about the field. Our observation of the negative values of the Wigner function

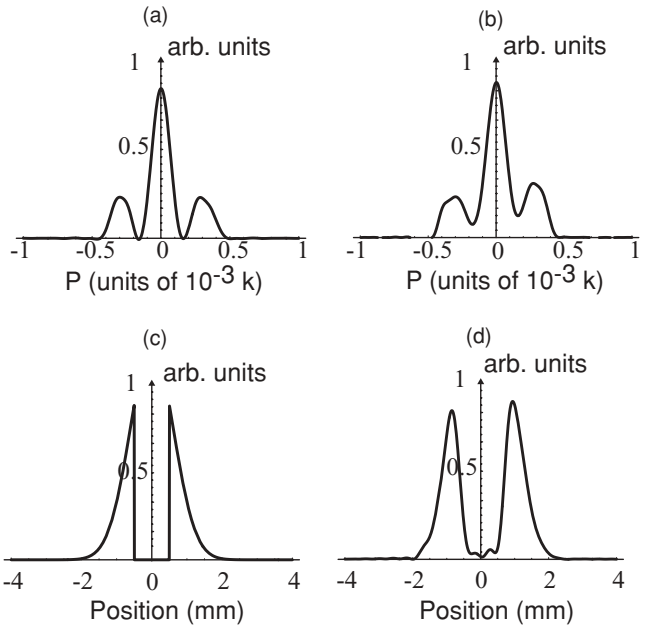

FIG. 13. The momentum and position distributions for the Schrödinger's cat state. (a) and (c) are the theoretical prediction of momentum and position distributions of the cat state. (b) and (d) are the corresponding experimental results of momentum and position distribution of the cat state obtained by integrating the reconstructed Wigner function over x and p, respectively.

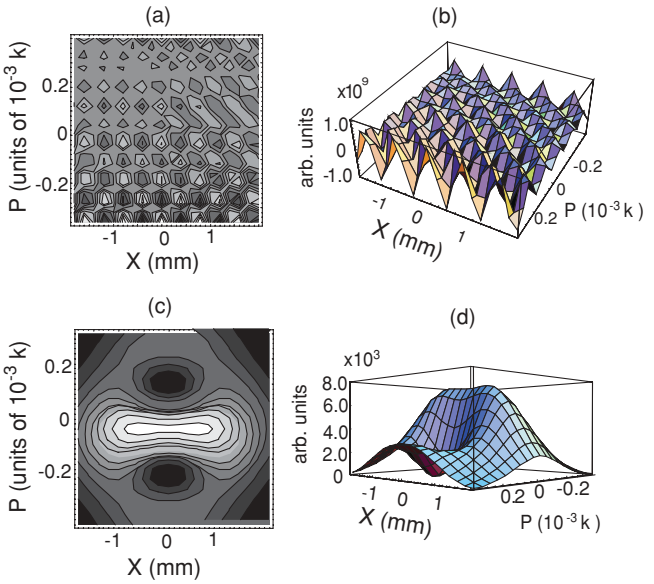

FIG. 14. (Color online) The reconstructed P distribution (a) 2D plot (b) 3D plot, and the Q distribution (c) 2D plot (d) 3D plot for slightly displaced coherent beams.

for this coherent field does not claim that the negative values exhibited by a quantum field are not a quantum feature. We believe that classical or quantum features of an experiment are based on classical or quantum fields involved in the experiment.

From the obtained Wigner function, one can obtain the position and momentum distribution of the $\mathcal{E}_s(x)$ by using the formulas $|\mathcal{E}_S(p)|^2 = \int_{-\infty}^{\infty} W_S(x,p)dx$ and $|\mathcal{E}_S(x)|^2 = \int_{-\infty}^{\infty} W_S(x,p)dp$ as shown in Figs. 13(b) and 13(d), respectively. The resolution of these plots is better than Figs. 10 and 11 because we numerically generate more data points from the reconstructed Wigner function. The measurements are in agreement with the theoretical predictions as shown in Figs. 13(a) and 13(c), respectively.

As discussed previously, we first obtain the characteristic function $\mathcal{M}_{\mathrm{KR}}(x',p')$ and then the P and Q distributions for this signal field. These distributions are plotted in Fig. 14. The Q distribution exhibits the broadening or low resolution of phase-space features compared to the Wigner function. While the P distribution is not a well behaved function for this field as it is expected for a P distribution.

V. DISCUSSION AND CONCLUSION

Spatial properties of the photon wave mechanics approach [25] for a single photon have been studied in detail. The approach can be applied to both the single-photon state and coherent field. As a consequence, the coherent field is the best testing ground for developing the tomography method for quantum information processing. In similar efforts, coherent fields have played an important role in quantum communication and computing such as the search algorithm [47–50] and factorization of numbers [51]. Optical wave mechanics implementations [52,53] of entanglement and superposition with coherent fields (coherent state with large photon numbers) have been demonstrated. This implementation has been used to study entanglement swapping and tests of nonlocality. However, the photon wave mechanic approach [25] for two-photon and multiphoton spatial qubits has not been relatively explored. The two-LO technique developed in this paper will provide another tomography tool to explore spatial qubits because it can provide local and nonlocal information of the wave field through the KR and Wigner distributions. In general, the particle-wave duality of a single-particle wave function can be represented by both distributions. However, we found that, based on our results on the superposition of two slightly displaced coherent beams, the phase-space interference of the Wigner distribution can clearly exhibit particle-wave duality of the wave field compared to the KR distribution. The local information of the wave field represented by the KR distribution, which did not exhibit phase-space interference, is useful to explore particle properties of the wave field.

We would like to discuss the KR and Wigner distributions separately because the local and nonlocal information of the wave field can provide independent useful information for quantum and coherent information processing including biomedical imaging [40].

Particle picture or local information of a wave field exhibited by the KR distribution in Fig. 9 has advantages in positioning or angle (momentum) resolving to extract local activities of an target. The method can directly locate the field or structure of an object without applying any raw data transformation. This will be particularly useful in cell tissue characterization such as prostate cancer cell detection. The KR distribution can be used to study Goos-Hanchen (GH) shifts [54] occurring in near-field optics and photonic waveguide. GH shifts in position and momentum can be used to identify the loss due to photonic crystal waveguide fabrication.

The wave picture or nonlocal information of a wave field as shown in Fig. 12 is best exhibited by the Wigner function. We observe the nonpositive properties of the Wigner function for a superposition of two spatially separated Gaussian fields $\mathcal{E}(x)$ analogous to a Schrödinger's cat state in a spatial coordinate. We have demonstrated the similarities in phase-space interference between spatial properties of quantum and coherent fields via the measurement of the Wigner function. We also show that an interesting analogy exists between our choice of LO field and that employed in the quantum-teleportation experiment [55]. In the x-p representation, the small and the large beams of our two-LO can be viewed as the superposition of the position (in-phase) and the momentum (out-of-phase) squeezed fields. A $\mathcal{E}(x)$ spatial Gaussian field of TEM_{00} is the lowest mode and is similar to a coherent state in the phase-space picture. Gaussian beams of smaller (larger) size than the lowest mode correspond to position (momentum) squeezed states. The two-LO technique here can only be used if we know the nominal size of the signal beam. The focused and collimated LO beams must be chosen to achieve sufficient x and p resolutions for the given signal beam. These are the similar problems encountered in our experiments and in the quantum-teleportation experiments which teleport an arbitrary state as a Wigner function via EPR beams [55].

In a complex multiparticle system or large-N biological system, we believe the KR and Wigner distributions are very useful to study the local and nonlocal information

of a macroscopic wave field such as the mechanisms of decoherence due to neighbor particles, quantum mapping of the*N*-particle system or semiclassical system, and macroscopic entanglement between two macroscopic mirrors.

In conclusion, we have demonstrated the direct measurement of the KR distribution using two-LO balanced heterodyne detection technique. The characteristic function of the KR is related to the Wigner, *P,* and *Q* distributions. Then the Wigner, *P,* and *Q* distributions are plotted by using raw data from the KR distribution. The physical properties of a wave field such as local and nonlocal phase-space information are illustrated through the KR and Wigner functions, respectively. This two-LO technique can be used in information processing including quantum information for quantum mapping and optical imaging for biomedical applications.

ACKNOWLEDGMENTS

The paper is prepared under the support of Michigan Tech's Start-up fund.

[1] K. F. Lee, F. Reil, S. Bali, A. Wax, and J. E. Thomas, Opt. Lett. **24**, 1370 (1999).
[2] A. Wax and J. E. Thomas, Opt. Lett. **21**, 1427 (1996).
[3] A. Wax, S. Bali, and J. E. Thomas, Phys. Rev. Lett. **85**, 66 (2000).
[4] F. Reil and J. E. Thomas, Phys. Rev. Lett. **95**, 143903 (2005).
[5] C. Iaconis and I. A. Walmsley, Opt. Lett. **21**, 1783 (1996).
[6] C. C. Cheng and M. G. Raymer, Phys. Rev. Lett. **82**, 4807 (1999).
[7] B. J. Smith, B. Killett, M. G. Raymer, I. A. Walmsley, and K. Banaszek, Opt. Lett. **30**, 3365 (2005).
[8] E. Mukamel, K. Banaszek, I. A. Walmsley, and C. Dorrer, Opt. Lett. **28**, 1317 (2003).
[9] J. G. Kirkwood, Phys. Rev. **44**, 31 (1933).
[10] E. P. Wigner, Phys. Rev. **40**, 749 (1932).
[11] A. N. Rihaczek, IEEE Trans. Inf. Theory **14**, 369 (1968).
[12] S. John, G. Pang, and Y. Yang, J. Biomed. Opt. **1**, 180 (1996).
[13] M. J. Bastiaans, Opt. Commun. **25**, 26 (1978).
[14] M. J. Bastiaans, *The Wigner Distribution-Theory and Applications in Signal Processing*, edited by W. Mecklenbrauker and F. Hlawatsch (Elsevier, New York, 1997), pp. 375–426.
[15] K. Vogel and H. Risken, Phys. Rev. A **40**, 2847 (1989).
[16] D. T. Smithey, M. Beck, M. G. Raymer, and A. Faridani, Phys. Rev. Lett. **70**, 1244 (1993).
[17] A. I. Lvovsky and M. G. Raymer, Rev. Mod. Phys. **81**, 299 (2009).
[18] M. G. Raymer, M. Beck, and D. F. McAlister, Phys. Rev. Lett. **72**, 1137 (1994).
[19] D. F. McAlister, M. Beck, L. Clarke, A. Meyer, and M. G. Raymer, Opt. Lett. **20**, 1181 (1995).
[20] M. Beck, M. G. Raymer, I. A. Walmsley, and V. Wong, Opt. Lett. **18**, 2041 (1993).
[21] Robert K. Tyson, *Principles of Adaptive Optics*, 2nd ed. (Academic Press, New York, 1998).
[22] K. E. Cahil and R. J. Glauber, Phys. Rev. **177**, 1882 (1969).
[23] E. C. G. Sudarshan, Phys. Rev. Lett. **10**, 277 (1963).
[24] K. Husimi, Proc. Phys. Math. Soc. Jpn. **22**, 264 (1940).
[25] B. J. Smith and M. G. Raymer, New J. Phys. **9**, 414 (2007).
[26] L. Praxmeyer and K. Wódkiewicz, Opt. Commun. **223**, 349 (2003).
[27] J. P. Dahl, H. Mack, A. Wolf, and W. P. Schleich, Phys. Rev. A **74**, 042323 (2006).
[28] K. Banaszek and K. Wodkiewicz, Phys. Rev. Lett. **82**, 2009 (1999).
[29] W. P. Schleich, *Quantum Optics in Phase Space* (Wiley, New York, 2001).
[30] F. Toscano, D. A. R. Dalvit, L. Davidovich, and W. H. Zurek, Phys. Rev. A **73**, 023803 (2006).
[31] W. H. Zurek, Nature (London) **412**, 712 (2001).
[32] R. Loudon, *The Quantum Theory of Light*, 3rd ed. (Oxford University, New York, 2000).
[33] M. I. Kolobov, *Quantum Imaging*, 1st ed. (Springer, New York, 2006).
[34] M. I. Kolobov, Rev. Mod. Phys. **71**, 1539 (1999).
[35] M. I. Kolobov and I. V. Sokolov, Sov. Phys. JETP **63**, 1105 (1986).
[36] M. I. Kolobov and I. V. Sokolov, Sov. Phys. JETP **69**, 1097 (1989).
[37] M. I. Kolobov and I. V. Sokolov, Phys. Lett. A **140**, 101 (1989).
[38] M. I. Kolobov and I. V. Sokolov, Opt. Spectrosc. **66**, 440 (1989).
[39] M. I. Kolobov and I. V. Sokolov, Europhys. Lett. **15**, 271 (1991).
[40] M. E. Brezinski and B. Liu, Phys. Rev. A **78**, 063824 (2008).
[41] K. Wagner, J. Janousek, V. Delaubert, H. Zou, C. Hard, N. Treps, J. F. Morizur, P. K. Lam, and H. A. Bachor, Science **321**, 541 (2008).
[42] J. P. Paz, A. J. Roncaglia, and M. Saraceno, Phys. Rev. A **69**, 032312 (2004).
[43] C. Miquel, J. P. Paz, and M. Saraceno, Phys. Rev. A **65**, 062309 (2002).
[44] L. Cohen, *Time-Frequency Analysis*, 1st ed. (Prentice Hall, Englewood Cliffs, NJ, 1994).
[45] W. H. Louisell, *Quantum Statistical Properties of Radiation*, 1st ed. (Wiley, New York, 1973).
[46] A. Wax, Ph.D. thesis, Duke University, 1999.
[47] S. Lloyd, Phys. Rev. A **61**, 010301(R) (1999).
[48] N. Bhattacharya, H. B. van Linden van den Heuvell, and R. J. Spreeuw, Phys. Rev. Lett. **88**, 137901 (2002).
[49] R. J. C. Spreeuw, Phys. Rev. A **63**, 062302 (2001).
[50] K. F. Lee, Opt. Lett. **34**, 1099 (2009).
[51] D. Bigourd, B. Chatel, W. P. Schleich, and B. Girard, Phys. Rev. Lett. **100**, 030202 (2008).
[52] K. F. Lee and J. E. Thomas, Phys. Rev. A **69**, 052311 (2004).
[53] K. F. Lee and J. E. Thomas, Phys. Rev. Lett. **88**, 097902 (2002).
[54] B. M. Jost, A.-A. R. Al Rashed, and B. E. A. Saleh, Phys. Rev. Lett. **81**, 2233 (1998).
[55] A. Furusawa, J. L. Sorensen, S. L. Braunstein, C. A. Fuchs, H. J. Kimble, and E. S. Polzik, Science **282**, 706 (1998).